Exact functional derivative of the nonadditive kinetic-energy bifunctional in the long-distance limit

Christoph R. Jacob,[a] S. Maya Beyhan,[b] and Lucas Visscher[c]
Department of Theoretical Chemistry, Faculty of Sciences, Vrije Universiteit Amsterdam, De Boelelaan 1083, 1081 HV Amsterdam, The Netherlands

(Received 15 March 2007; accepted 30 April 2007; published online 21 June 2007)

We have investigated the functional derivative of the nonadditive kinetic-energy bifunctional, which appears in the embedding potential that is used in the frozen-density embedding formalism, in the limit that the separation of the subsystems is large. We have derived an exact expression for this kinetic-energy component of the embedding potential and have applied this expression to deduce its exact form in this limit. Comparing to the approximations currently in use, we find that while these approximations are correct at the nonfrozen subsystem, they fail completely at the frozen subsystem. Using test calculations on two model systems, a $H_2O\cdots Li^+$ complex and a cluster of aminocoumarin C151 surrounded by 30 water molecules, we show that this failure leads to a wrong description of unoccupied orbitals, which can lead to convergence problems caused by too low-lying unoccupied orbitals and which can further have serious consequences for the calculation of response properties. Based on our results, a simple correction is proposed, and we show that this correction is able to fix the observed problems for the model systems studied. © *2007 American Institute of Physics*. [DOI: 10.1063/1.2743013]

I. INTRODUCTION

The frozen-density embedding (FDE) formalism within density functional theory[1,2] (DFT) offers an efficient scheme for the quantum chemical description of large systems by splitting the total system into an active subsystem and a frozen environment. In particular, for the description of solvent effects, this DFT-in-DFT embedding scheme has been shown to be both an accurate and an efficient method for the calculation of absorption spectra,[3–5] electron spin resonance parameters,[6] and nuclear magnetic resonance chemical shifts.[7] It has further been successfully applied to model more complex environments, e.g., for describing induced circular dichroism in host-guest systems[8] or for free-energy calculations in protein environments.[9,10] Recently, Neugebauer has extended the FDE formalism to describe couplings between electronic transitions in different subsystems.[11] In addition, it has been extended by Carter and co-workers to embed a system of interest, which is described using wave function based *ab initio* methods, in an environment described by DFT.[12–16]

The FDE scheme is based on a partitioning of the electron density of the total system ρ_{tot} into the electron densities ρ_{I} and ρ_{II} of two appropriately chosen subsystems. These electron densities of the subsystems are each calculated separately, with the effect of the other subsystem represented by an effective embedding potential which only depends on its charge density. This embedding potential contains a component v_T that is given by the functional derivative of the nonadditive kinetic-energy bifunctional,

$$v_T[\rho_{\mathrm{I}},\rho_{\mathrm{II}}](\boldsymbol{r}) = \frac{\delta T_s^{\mathrm{nadd}}[\rho_{\mathrm{I}},\rho_{\mathrm{II}}]}{\delta\rho_{\mathrm{I}}} = \left.\frac{\delta T_s[\rho]}{\delta\rho}\right|_{\rho=\rho_{\mathrm{tot}}(\boldsymbol{r})} - \left.\frac{\delta T_s[\rho]}{\delta\rho}\right|_{\rho=\rho_{\mathrm{I}}(\boldsymbol{r})}, \tag{1}$$

where the nonadditive kinetic energy T_s^{nadd} is defined as

$$T_s^{\mathrm{nadd}}[\rho_{\mathrm{I}},\rho_{\mathrm{II}}] = T_s[\rho_{\mathrm{I}}+\rho_{\mathrm{II}}] - T_s[\rho_{\mathrm{I}}] - T_s[\rho_{\mathrm{II}}]. \tag{2}$$

In the above expressions, $T_s[\rho]$ is the kinetic energy of the noninteracting reference system, as it is defined within Kohn-Sham (KS) DFT, which is usually calculated using the KS orbitals.

However, with the given partitioning into subsystems, the KS orbitals are only available for the subsystems and not for the full system, and $T_s[\rho_{\mathrm{I}}+\rho_{\mathrm{II}}]$ can therefore not be calculated directly. For this reason, in practical applications approximations have to be introduced in the construction of the kinetic-energy component $v_T[\rho_{\mathrm{I}},\rho_{\mathrm{II}}]$ of the embedding potential. Up to now, only approximations of the form

$$\tilde{v}_T[\rho_{\mathrm{I}},\rho_{\mathrm{II}}](\boldsymbol{r}) = \left.\frac{\delta \tilde{T}_s[\rho]}{\delta\rho}\right|_{\rho=\rho_{\mathrm{tot}}(\boldsymbol{r})} - \left.\frac{\delta \tilde{T}_s[\rho]}{\delta\rho}\right|_{\rho=\rho_{\mathrm{I}}(\boldsymbol{r})} \tag{3}$$

have been applied, where the tilde is used to label approximate quantities and $\tilde{T}_s[\rho]$ refers to some approximate kinetic-energy functional. The simplest approximation for the kinetic-energy functional, corresponding to the local-density approximation (LDA), is the well-known Thomas-Fermi functional, and a large number of more advanced approximate kinetic-energy functionals are available (for an overview see, e.g., Refs. 17 and 18).

For their application in calculations using the FDE scheme, different generalized-gradient approximation (GGA)

[a]Electronic mail: jacob@few.vu.nl
[b]Electronic mail: mbeyhan@few.vu.nl
[c]Electronic mail: visscher@chem.vu.nl

kinetic-energy functionals have been tested and compared for a number of weakly interacting systems.[19–21] Based on these results, a large number of studies employing the FDE scheme have been conducted using the PW91k kinetic-energy functional, which is a GGA functional using the same analytic form of the enhancement factor as the exchange functional of Perdew and Wang,[22] but that has been reparametrized for the kinetic energy by Lembarki and Chermette.[23]

The approximation of $v_T[\rho_I, \rho_{II}]$ using Eq. (3) in combination with the PW91k kinetic-energy functional has been shown to yield reliable results in FDE calculations in a number of studies. In particular, it has been found to be accurate in studies of weakly interacting complexes[24–27] and of solvent effects on different molecular properties.[3–5,7] However, the applicability of the currently available kinetic-energy functional is limited to systems where the interaction between the two subsystems is not too strong. While accurate results can be obtained for van der Waals complexes as well as for hydrogen-bound systems, a description of stronger interactions such as chemical bonds is not possible. It thus remains a challenge to develop approximations to $v_T[\rho_I, \rho_{II}]$ that are applicable also in the case of stronger interactions.

Also, in the case of weaker interactions the currently available kinetic-energy functionals need improvements for certain applications. Iannuzzi *et al.* have made use of FDE for molecular dynamics simulations in the condensed phase,[28] but have found that with the available LDA and GGA kinetic-energy functionals, they were not able to describe water at ambient conditions correctly. The pair distribution functions they obtained showed only an unstructured second solvation shell, and they attributed this wrong description to shortcomings of the approximate kinetic-energy functional.

Furthermore, for weakly interacting complexes an "electron-leak" problem in FDE calculations has been discussed. Near the nuclei in the frozen subsystem, the attractive nuclear potential is very large and, when using LDA or GGA kinetic-energy functionals, the kinetic-energy component of the embedding potential is not able to completely compensate this attraction. This might lead to electrons of the nonfrozen system leaking to the nuclei of the frozen subsystem, causing an artificial charge transfer between the subsystems. This problem has first been discussed for a complex of a fluorine anion and a water molecule at short distances by Stefanovich and Truong,[29] who proposed the use of a pseudopotential representing the core orbitals to overcome this problem. However, Dulak and Wesolowski reinvestigated this electron-leak problem for $F^-\cdots H_2O$ and $Li^+\cdots OH_2$ and found that at short distances it is of no importance for the calculation of the ground-state density and interaction energies.[30] On the other hand, in calculations on $CO_2\cdots X$ (X=He, Ne, Ar, Kr, Xe, and Hg) van der Waals complexes, it was found that for the complexes containing the heavier rare gases or mercury the dipole moment is overestimated if basis functions on the frozen system are included. This has also been attributed to the fact that close to the nuclei the PW91k kinetic-energy functional is not able to compensate the large nuclear attraction.[26]

In order to devise more accurate approximations of the kinetic-energy component v_T of the embedding potential, we will in this work investigate v_T in the limit of large separation of the two subsystems. In the quest for more accurate approximate functionals, both for the exchange-correlation energy as well as for the kinetic energy, it is a widely followed and successfully applied strategy to use exact physical boundary conditions and/or the known behavior in simple limiting cases. These can be used as guidance in the construction of approximate functionals by requiring that the approximations obey these physical limits.

Following this strategy, several approximate exchange-correlation functionals have been constructed, e.g., the GGA functional PBE (Ref. 31) and the meta-GGA functional TPSS.[32] Furthermore, exchange-correlation potentials have been constructed that have the correct asymptotic behavior far from the nuclei, which is particularly important for describing response properties.[33,34] Also, for the construction of approximate kinetic-energy functionals, this strategy has been applied. One example is a class of functionals by Carter and co-workers that are constructed to yield exact results for the linear response of the uniform electron gas.[35–37]

Instead of looking at the kinetic-energy functional itself, in this work we will focus on the quantity of interest directly, which is, in the case of the FDE scheme, the kinetic-energy component v_T of the embedding potential. As we will show, in the limit of large separation of the two subsystems, the two terms on the right-hand side of Eq. (1) do behave very differently in regions where either ρ_I or ρ_{II} are large, which can be used to deduce the exact v_T in this limit. It turns out that for regions where ρ_{II} is large, the available LDA or GGA kinetic-energy functionals do not obey this limit.

This work is organized as follows. After a brief review of FDE in Sec. II, we derive an expression for the exact nonadditive kinetic-energy potential in Sec. III. This is then used in Sec. IV to investigate the exact embedding potential at large separation of the two subsystems. After giving the computational details in Sec. V, we show in Sec. VI for model systems that the approximations currently in use for the kinetic-energy potential are not able to describe this long-distance limit correctly and investigate the consequences of this failure. In Sec. VII, a correction is proposed that enforces the correct embedding potential in the considered limit, before we summarize and conclude in Sec. VIII.

II. FROZEN-DENSITY EMBEDDING

In the FDE formalism[1,2] the total electron density $\rho_{tot}(\boldsymbol{r})$ is represented as the sum of two components $\rho_I(\boldsymbol{r})$ and $\rho_{II}(\boldsymbol{r})$. Usually, $\rho_I(\boldsymbol{r})$ and $\rho_{II}(\boldsymbol{r})$ are chosen to be either the electron densities of two interacting fragments of the considered system or as the electron densities of a system under investigation and an environment. In the latter case, the electron density of the environment is usually obtained using some approximate procedure, for instance, by using a sum of the electron densities of molecular fragments.[3,5]

Given this partitioning of the electron density, the DFT total energy can be expressed as a bifunctional of ρ_I and ρ_{II},

$$E[\rho_{\mathrm{I}},\rho_{\mathrm{II}}] = \int (\rho_{\mathrm{I}}(\boldsymbol{r}) + \rho_{\mathrm{II}}(\boldsymbol{r}))(v_{\mathrm{I}}^{\mathrm{nuc}}(\boldsymbol{r}) + v_{\mathrm{II}}^{\mathrm{nuc}}(\boldsymbol{r}))d\boldsymbol{r} + \frac{1}{2}\int \frac{(\rho_{\mathrm{I}}(\boldsymbol{r}) + \rho_{\mathrm{II}}(\boldsymbol{r}))(\rho_{\mathrm{I}}(\boldsymbol{r}') + \rho_{\mathrm{II}}(\boldsymbol{r}'))}{|\boldsymbol{r}-\boldsymbol{r}'|}d\boldsymbol{r}d\boldsymbol{r}' + E_{\mathrm{xc}}[\rho_{\mathrm{I}}+\rho_{\mathrm{II}}] + T_s[\rho_{\mathrm{I}}] + T_s[\rho_{\mathrm{II}}] + T_s^{\mathrm{nadd}}[\rho_{\mathrm{I}},\rho_{\mathrm{II}}], \tag{4}$$

where $v_{\mathrm{I}}^{\mathrm{nuc}}$ and $v_{\mathrm{II}}^{\mathrm{nuc}}$ are the electrostatic potentials of the nuclei in subsystems I and II, respectively, E_{xc} is the exchange-correlation functional, $T_s[\rho]$ is the kinetic energy of the noninteracting reference system, and $T_s^{\mathrm{nadd}}[\rho_{\mathrm{I}},\rho_{\mathrm{II}}]$ is the nonadditive kinetic-energy bifunctional.

For a given frozen electron density $\rho_{\mathrm{II}}(\boldsymbol{r})$ in one of the subsystems (fragment II), one can derive[1] one-electron equations for the calculation of the electron density $\rho_{\mathrm{I}}(\boldsymbol{r})$ in the other subsystem (fragment I) from the requirement that the total density $\rho_{\mathrm{tot}}(\boldsymbol{r})=\rho_{\mathrm{I}}(\boldsymbol{r})+\rho_{\mathrm{II}}(\boldsymbol{r})$ of the system is obtained, in an optimization process in which the electron density $\rho_{\mathrm{II}}(\boldsymbol{r})$ of fragment II is kept frozen. On the assumption that the complementary $\rho_{\mathrm{I}}(\boldsymbol{r})$ is positive definite and is noninteracting v_s-representable,[38] one obtains the Kohn-Sham equations with constrained electron density (KSCED),

$$\left[-\frac{\nabla^2}{2} + v_{\mathrm{eff}}^{\mathrm{KSCED}}[\rho_{\mathrm{I}},\rho_{\mathrm{II}}](\boldsymbol{r})\right]\phi_i(\boldsymbol{r}) = \epsilon_i\phi_i(\boldsymbol{r}), \quad i = 1,\ldots,\frac{N_{\mathrm{I}}}{2}, \tag{5}$$

from which the KS orbitals and the associated electron density of fragment I can be obtained.

The KSCED effective potential is given by

$$v_{\mathrm{eff}}^{\mathrm{KSCED}}[\rho_{\mathrm{I}},\rho_{\mathrm{II}}](\boldsymbol{r}) = v_{\mathrm{eff}}^{\mathrm{KS}}[\rho_{\mathrm{I}}](\boldsymbol{r}) + v_{\mathrm{eff}}^{\mathrm{emb}}[\rho_{\mathrm{I}},\rho_{\mathrm{II}}](\boldsymbol{r}), \tag{6}$$

where $v_{\mathrm{eff}}^{\mathrm{KS}}[\rho_{\mathrm{I}}](\boldsymbol{r})$ is the KS effective potential of the isolated subsystem I containing the usual terms of the nuclear potential, the Coulomb potential of the electrons, and the exchange-correlation potential,

$$v_{\mathrm{eff}}^{\mathrm{KS}}[\rho_{\mathrm{I}}](\boldsymbol{r}) = v_{\mathrm{I}}^{\mathrm{nuc}}(\boldsymbol{r}) + \int \frac{\rho_{\mathrm{I}}(\boldsymbol{r}')}{|\boldsymbol{r}-\boldsymbol{r}'|}d\boldsymbol{r}' + \left.\frac{\delta E_{\mathrm{xc}}[\rho]}{\delta\rho}\right|_{\rho=\rho_{\mathrm{I}}(\boldsymbol{r})}. \tag{7}$$

The effective embedding potential $v_{\mathrm{eff}}^{\mathrm{emb}}[\rho_{\mathrm{I}},\rho_{\mathrm{II}}](\boldsymbol{r})$ describes the interaction of the subsystem I with the frozen density of subsystem II and reads

$$v_{\mathrm{eff}}^{\mathrm{emb}}[\rho_{\mathrm{I}},\rho_{\mathrm{II}}](\boldsymbol{r}) = v_{\mathrm{II}}^{\mathrm{nuc}}(\boldsymbol{r}) + \int \frac{\rho_{\mathrm{II}}(\boldsymbol{r}')}{|\boldsymbol{r}-\boldsymbol{r}'|}d\boldsymbol{r}' + \left.\frac{\delta E_{\mathrm{xc}}[\rho]}{\delta\rho}\right|_{\rho=\rho_{\mathrm{tot}}(\boldsymbol{r})} - \left.\frac{\delta E_{\mathrm{xc}}[\rho]}{\delta\rho}\right|_{\rho=\rho_{\mathrm{I}}(\boldsymbol{r})} + v_T[\rho_{\mathrm{I}},\rho_{\mathrm{II}}](\boldsymbol{r}), \tag{8}$$

where the kinetic-energy part $v_T[\rho_{\mathrm{I}},\rho_{\mathrm{II}}]$ of the KSCED effective potential is given as the functional derivative of the nonadditive kinetic-energy bifunctional,

$$v_T[\rho_{\mathrm{I}},\rho_{\mathrm{II}}](\boldsymbol{r}) = \frac{\delta T_s^{\mathrm{nadd}}[\rho_{\mathrm{I}},\rho_{\mathrm{II}}]}{\delta\rho_{\mathrm{I}}} = \left.\frac{\delta T_s[\rho]}{\delta\rho}\right|_{\rho=\rho_{\mathrm{tot}}(\boldsymbol{r})} - \left.\frac{\delta T_s[\rho]}{\delta\rho}\right|_{\rho=\rho_{\mathrm{I}}(\boldsymbol{r})}. \tag{9}$$

Since the KSCED effective potential $v_{\mathrm{eff}}^{\mathrm{KSCED}}[\rho_{\mathrm{I}},\rho_{\mathrm{II}}](\boldsymbol{r})$ in Eq. (5) depends on both the density of the nonfrozen subsystem I and the density of the frozen subsystem, the KSCED equations have to be solved self-consistently. It should be noted that in contrast to the bifunctional of the nonadditive kinetic energy of Eq. (2), v_T is not symmetric with respect to the exchange of the two electron densities, i.e., $v_T[\rho_{\mathrm{I}},\rho_{\mathrm{II}}] \neq v_T[\rho_{\mathrm{II}},\rho_{\mathrm{I}}]$. Since the kinetic energy T_s does not depend on the electron density directly but on the KS orbitals (which, in turn, depend on the electron density), the evaluation of the functional derivative $\delta T_s[\rho]/\delta\rho$ is not possible in a straightforward way.

III. THE EXACT NONADDITIVE KINETIC-ENERGY POTENTIAL

The calculation of the kinetic-energy component $v_T[\rho_{\mathrm{I}},\rho_{\mathrm{II}}](\boldsymbol{r})$ of the KSCED effective potential requires the evaluation of the functional derivative $\delta T_s[\rho]/\delta\rho$ for two different electron densities—for the density of the nonfrozen subsystem I and for the total electron density. In this section we will first describe a general procedure for the evaluation of $\delta T_s[\rho]/\delta\rho$ for an arbitrary v_s-representable electron density.

The functional derivative of the nonadditive kinetic-energy bifunctional with respect to the electron density cannot be evaluated directly since the noninteracting kinetic energy does not depend directly on the density, but it requires the knowledge of the KS orbitals. The KS orbitals are an implicit functional of the electron density because the electron density uniquely defines a corresponding KS potential $v_s[\rho]$, which, in turn, determines the KS orbitals. The usual method for the evaluation of the functional derivative of orbital-dependent functionals is the optimized effective potential (OEP) method.[39]

However, in the case of the kinetic energy an alternative route is possible for the evaluation of $\delta T_s[\rho]/\delta\rho$. For an arbitrary v_s-representable electron density $\rho(\boldsymbol{r})$ there exists the corresponding KS potential $v_s[\rho](\boldsymbol{r})$, i.e., the potential that will yield the density $\rho(\boldsymbol{r})$. The existence of this one-to-one mapping between the electron density and the KS potential is given by the first Hohenberg-Kohn theorem.[38,40] Throughout this paper, we use $v_s[\rho]$ to refer to this KS potential, yielding the density $\rho(\boldsymbol{r})$. This is to be distinguished from the KS effective potential $v_{\mathrm{eff}}^{\mathrm{KS}}[\rho]$ that can be calculated from the electron density ρ according to Eq. (7). Only for the ground-state electron density $\rho_0(\boldsymbol{r})$, which can be obtained from the self-consistent solution of the KS equations, $v_s[\rho_0]$ and $v_{\mathrm{eff}}^{\mathrm{KS}}[\rho_0]$ are identical. For the practical evaluation of $v_s[\rho]$ from a given density $\rho(\boldsymbol{r})$, there are different numerical schemes available.[33,41,42]

To evaluate the functional derivative $\delta T_s[\rho]/\delta\rho$, we will consider this KS potential $v_s^{\rho}(\boldsymbol{r})$ as fixed by the given input density; i.e., the functional dependence on $\rho(\boldsymbol{r})$ is replaced by

a parametrical dependence. For this fixed potential $v_s^\rho(\boldsymbol{r})$, the electron density $\rho(\boldsymbol{r})$ is the density which minimizes the total-energy functional

$$E_{v_s^\rho}[\rho] = T_s[\rho] + \int v_s^\rho(\boldsymbol{r})\rho(\boldsymbol{r})d\boldsymbol{r} \tag{10}$$

of a system of noninteracting electrons with $v_s^\rho(\boldsymbol{r})$ as the external potential under the constraint that the electron density integrates to the correct number of electrons. Therefore, the electron density $\rho(\boldsymbol{r})$ is the solution of the Lagrange minimization problem[38]

$$\delta\left\{E_{v_s^\rho}[\rho] - \mu^\rho\left(\int \rho(\boldsymbol{r})d\boldsymbol{r} - N\right)\right\} = 0, \tag{11}$$

which is equivalent to the Euler-Lagrange equation

$$\mu^\rho = \frac{\delta E_{v_s^\rho}[\rho]}{\delta\rho(\boldsymbol{r})} = \frac{\delta T_s[\rho]}{\delta\rho(\boldsymbol{r})} + v_s^\rho(\boldsymbol{r}), \tag{12}$$

where μ^ρ is a constant that depends on the input electron density and that can be identified to equal the orbital energy of the highest occupied molecular orbital (HOMO) in the exact functional limit.[43]

This Euler-Lagrange equation with the potential $v_s^\rho(\boldsymbol{r})$ holds for the given electron density $\rho(\boldsymbol{r})$, and it can be employed to evaluate the functional derivative of the noninteracting kinetic energy $\delta T_s[\rho]/\delta\rho$ from

$$\frac{\delta T_s[\rho]}{\delta\rho(\boldsymbol{r})} = -v_s^\rho(\boldsymbol{r}) + \mu^\rho. \tag{13}$$

When solving the KSCED equations, the above functional derivative is needed for two different electron densities, for the electron density of the nonfrozen subsystem $\rho_\mathrm{I}(\boldsymbol{r})$, and for the total electron density $\rho_\mathrm{tot}(\boldsymbol{r})$. Using the obtained expression for $\delta T_s[\rho]/\delta\rho$, the kinetic-energy component of the KSCED effective potential [Eq. (1)] can be written as

$$\begin{aligned} v_T[\rho_\mathrm{I},\rho_\mathrm{II}](\boldsymbol{r}) &= \frac{\delta T_s^\mathrm{nadd}[\rho_\mathrm{I},\rho_\mathrm{II}]}{\delta\rho_\mathrm{I}} \\ &= v_s[\rho_\mathrm{I}](\boldsymbol{r}) - v_s[\rho_\mathrm{tot}](\boldsymbol{r}) + \Delta\mu. \end{aligned} \tag{14}$$

In this expression $\Delta\mu = \mu^{\rho_\mathrm{I}} - \mu^{\rho_\mathrm{tot}}$ is a constant shift of the potential that leads to a constant shift in the orbital energies but that will effect neither the obtained orbitals nor the orbital energy differences. Therefore, the shift $\Delta\mu$ can be ignored in the following.

The above expression for $v_T[\rho_\mathrm{I},\rho_\mathrm{II}]$ can be employed for arbitrary pairs of v_s-representable electron densities ρ_I and ρ_tot and can, in principle, be used to evaluate the exact contribution of the nonadditive kinetic energy to the effective embedding potential during the solution of the KSCED equations. However, it requires the knowledge of the KS potentials corresponding to ρ_I and to ρ_tot, respectively. Those are, in general, not easy to obtain in practical calculations. The application of Eq. (14) for the calculation of the exact embedding potential will be the subject of our future work. In the present work, we will employ it to investigate $v_T[\rho_\mathrm{I},\rho_\mathrm{II}]$ in the long-distance limit without actually reconstructing KS potentials from the electron density.

IV. EXACT EFFECTIVE EMBEDDING POTENTIAL IN THE LONG-DISTANCE LIMIT

In the following, the effective embedding potential will be investigated in the limit of a large separation of the two subsystems. This limit will be referred to as the "long-distance limit." In this considered limit, the overlap of the electron densities of the two subsystems will be very small, and at every point in space $\boldsymbol{r}$,

$$\rho_\mathrm{tot}(\boldsymbol{r}) \approx \rho_\mathrm{I}(\boldsymbol{r}) \vee \rho_\mathrm{tot}(\boldsymbol{r}) \approx \rho_\mathrm{II}(\boldsymbol{r}). \tag{15}$$

This implies that also the corresponding KS potentials do not "overlap;" that is, at every point in space $\boldsymbol{r}$,

$$v_s[\rho_\mathrm{tot}](\boldsymbol{r}) \approx v_s[\rho_\mathrm{I}](\boldsymbol{r}) \vee v_s[\rho_\mathrm{tot}](\boldsymbol{r}) \approx v_s[\rho_\mathrm{II}](\boldsymbol{r}), \tag{16}$$

where we assumed that both $v_s[\rho_\mathrm{I}](\boldsymbol{r})$ and $v_s[\rho_\mathrm{II}](\boldsymbol{r})$, and therefore also $v_s[\rho_\mathrm{tot}](\boldsymbol{r})$, have been chosen such that they go to 0 at infinity, i.e., where the corresponding density approaches 0.

In addition, we will assume that the electron density ρ_II of the frozen subsystem in the environment is close to the correct total density, i.e., that the chosen partitioning of the electron density is such that the subsystem densities are equal to the ground-state densities of the separated subsystems. This restriction rules out the case where there is a charge transfer between the subsystems. Even though this is a quite severe restriction, this is the most common use of the FDE scheme. In most practical applications, an approximate $\rho_\mathrm{II}(\boldsymbol{r})$ is used, which is chosen such that it can be considered a good approximation to the correct electron density in the environment.

It should be noted that in the following "exact" effective embedding potential refers to the embedding potential that is constructed using the exact kinetic-energy component v_T. This does not require that also the exact exchange-correlation potential is used, but approximate exchange-correlation potentials can be employed. However, when using the exact embedding potential, the results of a fully variational FDE calculation (in which the electron density of both subsystems is updated in freeze-and-thaw cycles) will be equal to the electron density calculated from a supermolecular KS-DFT calculation using the same approximate exchange-correlation potential. In the following, we will restrict ourselves to approximate exchange-correlation potentials that only depend on the electron density locally, i.e., to LDA and GGA functionals.

Under these assumptions, the KS potential that yields the correct total electron density can, in the long-distance limit, be decomposed as

$$v_s[\rho_\mathrm{tot}](\boldsymbol{r}) \approx v_s[\rho_\mathrm{I}](\boldsymbol{r}) + v_s[\rho_\mathrm{II}](\boldsymbol{r}); \tag{17}$$

i.e., it can be written as the sum of the KS potentials that correspond to the individual electron densities of the subsystems. It should be pointed out that this decomposition is

only exact if approximate exchange-correlation potentials that only depend locally on the electron-density are employed. It is not valid if the exact KS potentials are considered.

A. Embedding potential at the nonfrozen subsystem

In the region of the nonfrozen subsystem I, where ρ_{II} is negligibly small $[\rho_{II}(\boldsymbol{r}) \approx 0]$, the total density equals the density of the nonfrozen subsystem I, i.e., $\rho_I(\boldsymbol{r}) \approx \rho_{tot}(\boldsymbol{r})$. This implies, under the assumptions made above, that

$$v_s[\rho_{tot}](\boldsymbol{r}) \approx v_s[\rho_I](\boldsymbol{r}), \tag{18}$$

and it follows from Eq. (14) that

$$v_T[\rho_I, \rho_{II}](\boldsymbol{r}) \approx 0 \quad \text{for} \quad \rho_{II}(\boldsymbol{r}) \approx 0; \tag{19}$$

i.e., the kinetic-energy component of the effective embedding potential disappears.

If a local approximation (LDA or GGA) to the exchange-correlation potential is used, also the exchange-correlation component of the effective embedding potential in Eq. (8) cancels, and the effective embedding potential reduces to the purely electrostatic embedding potential,

$$v_{eff}^{emb}[\rho_I, \rho_{II}](\boldsymbol{r}) = v_{II}^{nuc}(\boldsymbol{r}) + \int \frac{\rho_{II}(\boldsymbol{r}')}{|\boldsymbol{r} - \boldsymbol{r}'|} d\boldsymbol{r}' \quad \text{for} \quad \rho_{II}(\boldsymbol{r}) \approx 0. \tag{20}$$

B. Embedding potential at the frozen subsystem

In the region of the frozen subsystem II, where ρ_I is negligibly small $[\rho_I(\boldsymbol{r}) \approx 0]$, the total density equals the density of the frozen subsystem II, i.e., $\rho_{II}(\boldsymbol{r}) \approx \rho_{tot}(\boldsymbol{r})$. This implies, under the assumptions made above, that

$$v_s[\rho_{tot}](\boldsymbol{r}) \approx v_s[\rho_{II}](\boldsymbol{r}) \tag{21}$$

and

$$v_s[\rho_I](\boldsymbol{r}) \approx 0, \tag{22}$$

and it follows from Eq. (14) that

$$v_T[\rho_I, \rho_{II}](\boldsymbol{r}) \approx - v_s[\rho_{II}](\boldsymbol{r}) \quad \text{for} \quad \rho_I(\boldsymbol{r}) \approx 0. \tag{23}$$

As the frozen density $\rho_{II}(\boldsymbol{r})$ has usually been obtained from the self-consistent solution of the KS equations in an earlier step, the corresponding KS potential $v_s[\rho_{II}](\boldsymbol{r})$ is known and is given by the effective potential that was used to obtain $\rho_{II}(\boldsymbol{r})$. In the simplest case, ρ_{II} has been obtained from an isolated KS-DFT calculation. In this case, the KS potential corresponding to $\rho_{II}(\boldsymbol{r})$ is given by

$$v_s[\rho_{II}](\boldsymbol{r}) = v_{eff}^{KS}[\rho_{II}](\boldsymbol{r}) = v_{II}^{nuc}(\boldsymbol{r}) + \int \frac{\rho_{II}(\boldsymbol{r}')}{|\boldsymbol{r} - \boldsymbol{r}'|} d\boldsymbol{r}' + \left. \frac{\delta E_{xc}[\rho]}{\delta \rho} \right|_{\rho = \rho_{II}(\boldsymbol{r})}, \tag{24}$$

and, therefore,

$$v_T[\rho_I, \rho_{II}](\boldsymbol{r}) \approx - v_{II}^{nuc}(\boldsymbol{r}) - \int \frac{\rho_{II}(\boldsymbol{r}')}{|\boldsymbol{r} - \boldsymbol{r}'|} d\boldsymbol{r}' - \left. \frac{\delta E_{xc}[\rho]}{\delta \rho} \right|_{\rho = \rho_{II}(\boldsymbol{r})} \quad \text{for} \quad \rho_I(\boldsymbol{r}) \approx 0. \tag{25}$$

The nuclear potential and the electrostatic potential of the electrons exactly cancel the corresponding terms in the effective embedding potential [Eq. (8)], and in the case of a local approximation (LDA or GGA) for the exchange-correlation potential, the exchange-correlation component cancels, too. Therefore, the kinetic-energy component cancels all the other terms of v_{eff}^{emb}, and one obtains

$$v_{eff}^{emb}[\rho_I, \rho_{II}](\boldsymbol{r}) = 0 \quad \text{for} \quad \rho_I(\boldsymbol{r}) \approx 0. \tag{26}$$

If the frozen density ρ_{II} has not been obtained from an isolated molecule calculation, but from a FDE calculation itself, as it is done when performing freeze-and-thaw cycles, the KS potential corresponding to $\rho_{II}(\boldsymbol{r})$ also contains the effective embedding potential, i.e.,

$$v_s[\rho_{II}](\boldsymbol{r}) = v_{eff}^{KS}[\rho_{II}](\boldsymbol{r}) + v_{eff}^{emb}[\rho_{II}, \rho_I](\boldsymbol{r}), \tag{27}$$

where $v_{eff}^{emb}[\rho_{II}, \rho_I](\boldsymbol{r})$ is the embedding potential that appears when ρ_{II} is calculated in a FDE calculation in the presence of the (frozen) ρ_I density, i.e., when the roles of ρ_I and ρ_{II} are interchanged in a freeze-and-thaw calculation.

Since the distance between the two subsystems is large, the effective embedding potential in the calculation of ρ_{II} is, as described above in Sec. IV A, in the regions of interest given by the electrostatic potential only. Therefore,

$$v_T[\rho_I, \rho_{II}](\boldsymbol{r}) \approx - v_{eff}^{KS}[\rho_{II}](\boldsymbol{r}) - v_I^{nuc}(\boldsymbol{r}) - \int \frac{\rho_I(\boldsymbol{r}')}{|\boldsymbol{r} - \boldsymbol{r}'|} d\boldsymbol{r}' \quad \text{for} \quad \rho_I(\boldsymbol{r}) \approx 0. \tag{28}$$

The effective embedding potential at the frozen system is then given by

$$v_{eff}^{emb}[\rho_I, \rho_{II}](\boldsymbol{r}) = - v_I^{nuc}(\boldsymbol{r}) - \int \frac{\rho_I(\boldsymbol{r}')}{|\boldsymbol{r} - \boldsymbol{r}'|} d\boldsymbol{r}' \quad \text{for} \quad \rho_I(\boldsymbol{r}) \approx 0. \tag{29}$$

This effective embedding potential cancels the corresponding terms in the KS effective potential of the embedded subsystem $v_{eff}^{KS}[\rho_I]$, so that the total effective potential used in the calculation of the embedded subsystem is zero at the frozen subsystem,

$$v_{eff}^{KSCED}[\rho_I](\boldsymbol{r}) \approx 0 \quad \text{for} \quad \rho_I(\boldsymbol{r}) \approx 0. \tag{30}$$

V. COMPUTATIONAL DETAILS

All density functional calculations have been performed using the Amsterdam density functional (ADF) package.[44,45] The FDE scheme of Wesolowski and Warshel[1] has been implemented in the most recent version of ADF using an efficient numerical integration scheme.[4] The PW91 exchange-correlation functional,[22,46] in combination with the TZ2P basis set from the ADF basis set library,[44] has been employed in all calculations. If not stated otherwise, in the FDE calculations the PW91k kinetic-energy functional[23] has been used to

approximate the kinetic-energy component of the embedding potential according to Eq. (3). The calculations on $H_2O\cdots Li^+$ presented below have been independently verified using the implementation of the FDE scheme in the deMon2k program package.[47]

In the FDE calculations, there are two possibilities for the choice of the basis functions which are used to expand the density of the nonfrozen subsystems.[20,26] The most obvious choice is to use only basis functions that are centered on the atoms in the considered subsystem to expand the corresponding density. Calculations using this monomolecular basis set expansion will be labeled as FDE(m). However, in this case an inconsistency with respect to the supermolecular calculation is introduced since the products of basis functions of different subsystems cannot be used for expanding the electron density. Therefore, it is more accurate to include all basis functions, also those of the frozen subsystem, in the FDE calculation. Calculations using this supermolecular basis set expansion will be labeled as FDE(s).

VI. THE FAILURE OF THE AVAILABLE APPROXIMATE KINETIC-ENERGY POTENTIALS IN THE LONG-DISTANCE LIMIT

The currently available approximations to the kinetic-energy component v_T of the embedding potential, which are of the form

$$\tilde{v}_T[\rho_I,\rho_{II}](\boldsymbol{r}) = \left.\frac{\delta \tilde{T}_s[\rho]}{\delta\rho}\right|_{\rho=\rho_{tot}(\boldsymbol{r})} - \left.\frac{\delta \tilde{T}_s[\rho]}{\delta\rho}\right|_{\rho=\rho_I(\boldsymbol{r})}, \quad (31)$$

only partly satisfy the exact long-distance limit that was derived in the previous section. At the nonfrozen subsystem, $\rho_I(\boldsymbol{r}) \approx \rho_{tot}(\boldsymbol{r})$ and, therefore, the two terms in Eq. (31) will cancel, such that the correct long-distance limit given by Eq. (19) is obtained.

In contrast, at the frozen subsystem Eq. (31) reduces to

$$\tilde{v}_T[\rho_I,\rho_{II}](\boldsymbol{r}) = \left.\frac{\delta \tilde{T}_s[\rho]}{\delta\rho}\right|_{\rho=\rho_{II}(\boldsymbol{r})} \quad \text{for} \quad \rho_I(\boldsymbol{r}) \approx 0, \quad (32)$$

and it is not evident that the available kinetic-energy functionals fulfill the exact limit given by Eq. (23), i.e., that the kinetic-energy component cancels the electrostatic and exchange-correlation components of the effective embedding potential.

This wrong description of the long-distance limit can be considered a serious shortcoming of the approximate kinetic-energy functionals that are currently in use in practical applications of the FDE scheme. At the frozen system, the available approximate kinetic-energy functionals, used in Eq. (3) to approximate the kinetic-energy component v_T of the effective embedding potential, are in general not able to compensate the electrostatic parts of the embedding potential, as they should in the exact long-distance limit. We will investigate the consequences of this wrong description in the following.

To illustrate the behavior of the embedding potential in the different regions, we investigated a $H_2O\cdots Li^+$ complex as a simple model system. This complex has already been used in earlier studies of the possible charge-leak problem in FDE calculations.[29,30] The structure of this complex, as it was used in the calculations, is shown in Fig. 1. As a starting point, we use the optimized geometry of $H_2O\cdots Li^+$, which assumes a planar structure with C_{2v} symmetry and d(O–H) =0.97 Å, $\angle$(H–O–H)=105.1° and d(O–Li)=1.8 Å. To investigate the limit of large separations of the two subsystems, the O–Li distance is varied.

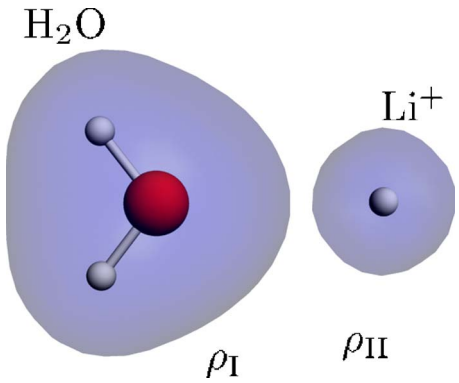

FIG. 1. (Color online) Structure of the employed model system $H_2O\cdots Li^+$. In the calculations the O–Li distance is varied; the picture is for d(O–Li) =5.8 Å. An isosurface plot of the electron density is also shown to illustrate the partitioning into subsystems. Graphics: ADF-VIEW (Ref. 54).

In the FDE calculations, the positively charged Li^+ ion is used as the frozen subsystem (ρ_{II}). The electron density of the Li^+ subsystem is calculated for the isolated ion in the gas phase. The H_2O molecule constitutes the nonfrozen subsystem (ρ_I), and its electron density is calculated in a FDE calculation in the presence of the frozen Li^+ electron density. At large separations, the effect of the H_2O subsystem on the Li^+ ion can be expected to be very small; i.e., the frozen Li^+ density will be very close to the correct total density, so that the assumptions made in Sec. IV are fulfilled. On the other hand, the effect of the frozen Li^+ subsystem can be expected to be significant even when the overlap of the electron densities is negligible since its positive charge gives rise to a long-range electrostatic interaction.

As a reference, we first performed supermolecular KS-DFT calculations. The orbital energies obtained in this supermolecular calculation as a function of the O–Li distance are shown in Fig. 2, and pictures of the relevant orbitals are

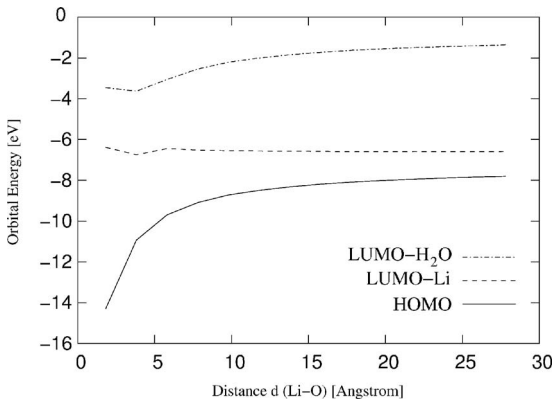

FIG. 2. Orbital energies calculated in a supermolecular KS-DFT calculation as a function of the O–Li distance. See text for details.

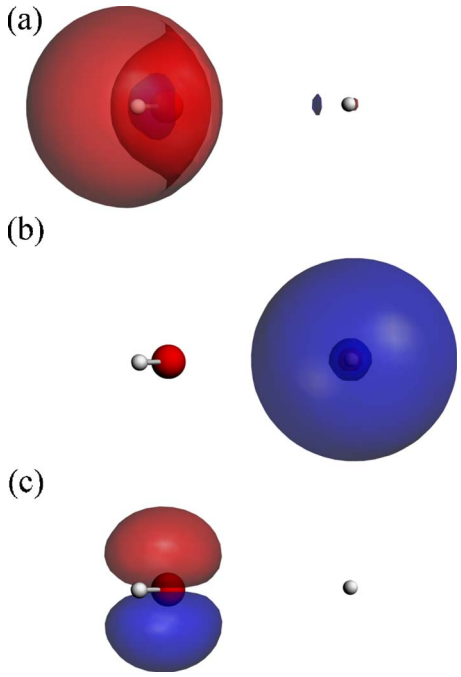

FIG. 3. (Color online) Isosurface plots of the orbitals calculated in a supermolecular KS-DFT calculation for d(O–Li)=5.8 Å. Shown are (a) the lowest unoccupied H_2O orbital (LUMO-H_2O), (b) the lowest unoccupied Li^+ orbital (LUMO-Li), and (c) the highest occupied H_2O orbital (HOMO-H_2O). See text for details. Graphics: ADF-VIEW (Ref. 54).

shown in Fig. 3.

The HOMO in the supermolecular calculation is a lone-pair p orbital on the water molecule. When the distance between the two fragments is increased, its orbital energy increases. This is due to the Coulomb potential of the charged Li^+ ion that is felt at the water molecule. The lowest unoccupied molecular orbital (LUMO) is the rather diffuse 2s orbital on the Li^+ ion (labeled LUMO-Li). Its orbital energy is almost constant with increasing distance between the fragments since at larger distances there is no interaction of this orbital with the H_2O molecule. Only close to the equilibrium distance there is some overlap of the LUMO-Li with H_2O orbitals. In addition, the figures also include the lowest unoccupied H_2O orbital, labeled LUMO-H_2O, i.e., the lowest unoccupied orbital that is mainly located at the H_2O molecule. This is a diffuse s-like orbital. As it is localized at the water molecule, its orbital energy shows the same Coulombic behavior as that of the HOMO when the distance between the fragments is increased.

The orbital energies of the HOMO and the LUMO in FDE calculations on the H_2O subsystem in the presence of the frozen Li^+ density, using both the monomolecular and the supermolecular expansion, are shown in Fig. 4. Pictures of the orbitals obtained with FDE(m) are shown in Fig. 5, and the orbitals calculated in the FDE(s) calculations are shown in Fig. 6.

Both in the FDE(m) and in the FDE(s) calculations the HOMO of the H_2O subsystem is the same orbital as the HOMO in the supermolecular calculation, and the orbital energy is identical to the orbital energy calculated in the supermolecular calculation. Since this orbital is localized at the H_2O subsystem, at larger separations of the two subsystems it is exposed to the embedding potential at the nonfrozen system only. As shown above, in these regions the embedding potential should reduce to the purely electrostatic embedding potential. With the approximate kinetic-energy functionals in use this limit is reproduced correctly.

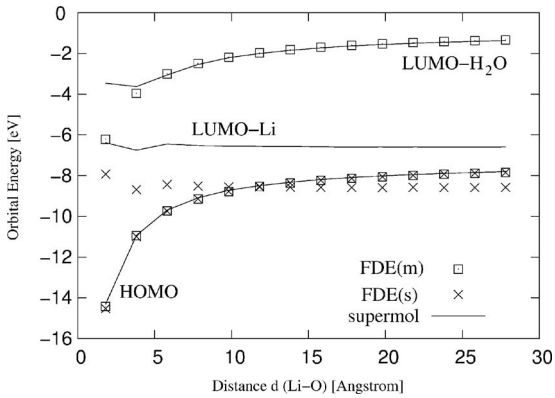

FIG. 4. Orbital energies calculated in FDE calculations on the H_2O subsystem in the presence of the frozen Li^+ subsystem as a function of the O–Li distance. Both results using the supermolecular basis set expansion [FDE(s)] and the monomolecular basis set expansion [FDE(m)] are shown. For comparison, also the corresponding supermolecular orbitals are included.

In the FDE(m) calculation the LUMO of the H_2O subsystem is at larger separations of the two subsystems similar to the LUMO-H_2O in the supermolecular calculation. It is a diffuse s-like orbital localized at the water subsystem. Therefore, it does not correspond to the LUMO of the supermolecule, but to the lowest unoccupied orbital of the subsystem in question. The orbital energy of the LUMO equals at larger distances the orbital energy of the LUMO-H_2O in the supermolecular calculation.

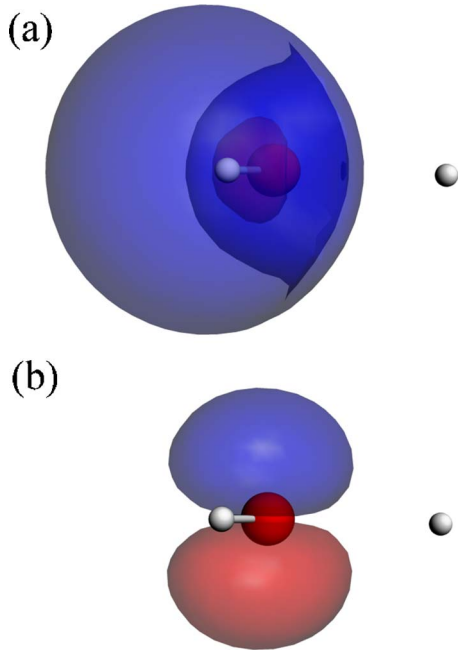

FIG. 5. (Color online) Isosurface plots of the H_2O orbitals calculated in a FDE(m) calculation in the presence of the frozen Li^+ subsystem for d(O–Li)=5.8 Å. Only basis functions of the H_2O subsystem are included (monomolecular expansion). Shown are (a) the lowest unoccupied molecular orbital and (b) the highest occupied molecular orbital. See text for details. Graphics: ADF-VIEW (Ref. 54).

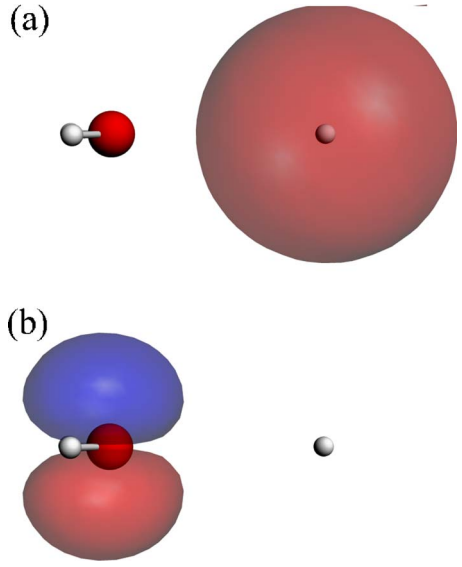

FIG. 6. (Color online) Isosurface plots of the H_2O orbitals calculated in a FDE(s) calculation in the presence of the frozen Li^+ subsystem for d(O–Li)=5.8 Å. Basis functions of both subsystems are used in the FDE calculation (supermolecular expansion). Shown are (a) the lowest unoccupied molecular orbital and (b) the highest occupied molecular orbital. See text for details. Graphics: ADF-VIEW (Ref. 54).

In the FDE(s) calculation, where the basis functions centered at the Li subsystem are included, a completely different orbital is found as the LUMO. In contrast to the FDE(m) calculation, where the LUMO was localized at the H_2O subsystem, a rather diffuse, nodeless s orbital localized at the Li^+ ion is obtained. The orbital energy of this orbital is at larger distances −8.6 eV, which is approximately 2.0 eV lower than the orbital energy of the LUMO-Li obtained in the supermolecular calculation. Since the orbital is localized at the Li^+ subsystem, its orbital energy is almost constant when the distance between the subsystems is increased. At O–Li distances larger than approximately 12 Å, the energy of the HOMO becomes larger than the orbital energy of the LUMO. In these cases the calculation has to be forced to converge to a nonaufbau solution.

The fact that a bound unoccupied orbital appears at the frozen subsystem is a consequence of the wrong limit of the kinetic-energy component of the embedding potential for the approximate kinetic-energy functional PW91k applied here. If the kinetic-energy component of the embedding potential shows the correct long-distance limit derived in Sec. IV B at the frozen system, the (repulsive) kinetic-energy component should cancel the attractive electrostatic potential. In this case, there should not be any bound orbitals localized at the frozen subsystem. The low-lying unoccupied orbital localized at the Li^+ subsystem is thus an artifact introduced by the use of an approximate kinetic-energy functional. The PW91k kinetic-energy functional is not able to compensate the attractive electrostatic parts of the embedding potential, which leads to an artificially too low-lying virtual orbital localized at the frozen subsystem. This wrong description is similar to the problems that arise if purely electrostatic models (e.g., point charges) are used to describe an environment, where additional measures, such as the introduction of pseudopotentials or a damping factor for the nuclear attraction, have to be taken to avoid the localization of charge on the environment.[48]

It should be noted that the limiting case for the embedding potential is quite different from the behavior that appears if a pseudopotential approach is used for representing the frozen subsystem, like it is, for instance, done in the effective group potential method.[49,50] In this case, only the occupied orbitals of the frozen subsystem are projected out of the variational space used for the nonfrozen system, so that all virtual orbitals present in the supermolecular calculation, including those localized at the frozen subsystem, will appear in the calculation on the nonfrozen subsystem. The partitioning of the electron density into the electron densities of subsystems that is the starting point for the FDE scheme leads to a partitioning not only of the occupied orbitals, but also implies a partitioning of the virtual orbital space. This is a consequence of the use of a local embedding potential that does not contain any projection operators, unlike in pseudopotential approaches.

To investigate the influence of the approximate kinetic-energy functional, we also performed calculations using the Thomas-Fermi (TF) functional to approximate the kinetic-energy component of the embedding potential. In this case, the general picture is identical to that obtained using PW91k, only that in the FDE(s) calculation the LUMO, which is also localized at the Li subsystem, has an even lower orbital energy. At larger distances, its orbital energy is approximately −8.7 eV, i.e., 2.1 eV lower than that of the LUMO-Li in the supermolecular calculation. Therefore, also when using the TF functional, the orbital energy of the artificially too low-lying LUMO is below the orbital energy of the HOMO, and a nonaufbau solution is obtained.

We did not investigate approximate GGA kinetic-energy functionals other than PW91k since only the TF functional and PW91k have been widely applied in practical applications of FDE. However, none of them ensures the correct long-distance limit. It can therefore be expected that any GGA kinetic-energy functional will behave similar to PW91k and show this shortcoming if applied for approximating the kinetic-energy component of the embedding potential.

Even though the failure of the kinetic-energy component of the embedding potential in the long-distance limit leads to artificially too low-lying unoccupied orbitals, it does not change the occupied orbitals since in the region of the nonfrozen subsystem the embedding potential is correct. Therefore, the calculated electron density will not be affected, as long as no orbital localized at the frozen subsystem is occupied and as long as there is no electron density leaking into the regions of the frozen system. However, the artificially too low-lying virtual orbitals will lead to a number of problems in practical applications of FDE.

First, as it was shown here in the case of $H_2O\cdots Li$, their orbital energies can be of similar size as the orbital energy of the HOMO of the nonfrozen system, or even drop below the orbital energy of the HOMO. This will lead to serious convergence problems since the self-consistent field procedure has to be forced to converge to a nonaufbau solution. Sec-

ond, the accurate description of virtual orbitals is crucial for the correct description of response properties such as excitation energies, which is a very important application of the FDE scheme.[3,4,8] In the calculation of response properties, the artificially too low-lying virtual orbitals will introduce spurious excitations to these orbitals. Even though they will, in general, have a low oscillator strength, they might mix with other excitations and thus influence the calculated absorption spectra.

In the FDE(m) calculations, the problem of artificially too low-lying virtual orbitals does not occur because there are no basis functions present that probe the regions of the frozen system, where the embedding potential is wrong. This might be a practical way of avoiding the problems discussed above. However, it does not solve them. Since FDE should be exact in the exact functional limit, it should also be applicable when larger basis sets are used. In many cases, it might be necessary to include basis functions on the frozen system, at least for a few atoms involved in (hydrogen) bonds with the nonfrozen subsystem because these basis functions are important to model the charge density in the bonding region.[20,51] Furthermore, the calculation of response properties of the nonfrozen subsystem often requires the use of basis sets containing very diffuse functions.[5] In calculations on weakly interacting systems such as van der Waals complexes the inclusion of diffuse functions is in many cases required.[26] These diffuse basis functions on the nonfrozen system will also probe the embedding potential at the frozen subsystem, thus possibly leading to artificially too low-lying virtual orbitals, even in FDE(m) calculations. In the examples presented here, the use of basis functions of the frozen subsystem would normally not be necessary, but they have been included to identify problems that will appear with sufficiently diffuse basis sets more clearly.

To demonstrate that the wrong long-distance limit of the kinetic-energy component v_T of the embedding potential does not only have consequences in rather artificial model systems, but also in cases that are of importance in practical applications, we have also investigated the system studied in Ref. 4, where solvent effects on the absorption spectrum of the organic dye aminocoumarin C151 have been studied. For our test calculations, we employed a cluster consisting of the aminocoumarin C151 molecule and the 30 closest solvent water molecules, using the coordinates of one arbitrary snapshot from the molecular dynamics simulation performed in Ref. 4. The structure of this cluster is shown in Fig. 7.

In the FDE calculations, the frozen subsystem is formed by the solvent environment, and a sum of the electron densities calculated for the isolated water molecules is used to approximate the frozen density ρ_{II}. For studying solvent effects it has been shown[3] that this is usually a good approximation to the true electron density of the solvent. It can, therefore, be assumed that this approximated density in the regions of the frozen density—at least in the regions where the overlap with the density of the nonfrozen subsystem is small—is close to the exact total density and that in these regions the assumptions made in Sec. IV are fulfilled.

The orbital energies of the four highest occupied MOs and of the unoccupied orbitals with orbital energies lower than −0.3 eV calculated for this test system are shown in Fig. 8. As a starting point, the orbitals calculated for the isolated aminocoumarin C151 are given. In this case, the virtual orbitals ($59a$–$62a$) are antibonding orbitals of the aminocoumarin C151. In the FDE(m) calculation, the orbital energies change significantly with respect to the isolated molecule calculation, which is due to the influence of the solvent environment. However, for both the occupied and the unoccupied orbitals in the energy range of interest, the main character of the orbitals does not change.

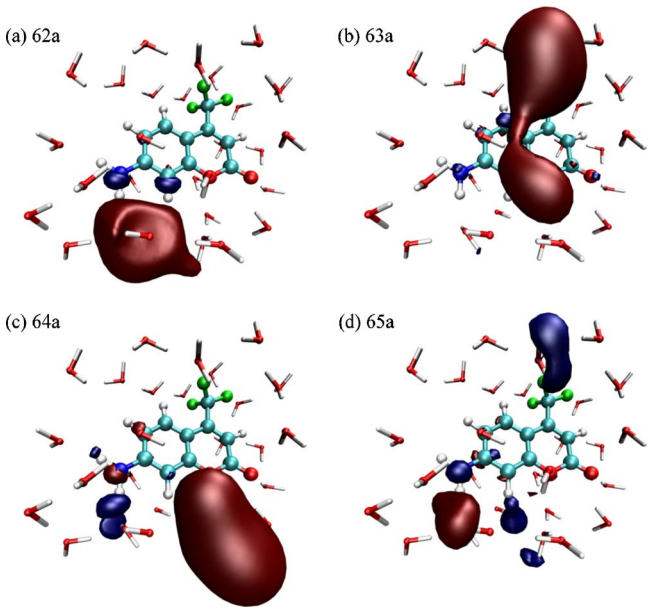

FIG. 7. (Color online) Structure of an aminocoumarin surrounded by 30 water solvent molecules and isosurface plots (contour value: 0.03) of the spurious unoccupied orbitals obtained in the FDE(s) calculation. See text for details. Graphics: VMD (Ref. 55).

In the FDE(s) calculations, the orbital energies of the orbitals $55a$–$61a$ are all slightly lower than in the FDE(m) calculation but do not change significantly. This can be attributed to the larger basis set available in the FDE(s) calculation. However, additional virtual orbitals ($62a$–$65a$) show up in the energy range of interest that were not present in the FDE(m) calculation. Isosurface plots of these unoccupied orbitals are shown in Fig. 7.

It can be seen that all four of these unoccupied orbitals are mainly localized at the water environment. As discussed above, these orbitals should not be present in the calculation of the aminocoumarin C151 subsystem. They are thus artificially too low-lying orbitals introduced by the wrong long-distance limit of the approximations used for the kinetic-energy component of the embedding potential. This shows that this wrong limit does also have consequences in realistic systems that have been studied using the FDE scheme if basis functions that can probe the regions of the frozen subsystem are present.

The artificially too low-lying virtual orbitals also show up in the calculation of the absorption spectrum by introducing spurious excitations. In the spectrum calculated using time dependent DFT (TDDFT), the seventh excitation has a contribution of 28.1% of an excitation from orbital $58a$ to orbital $63a$, i.e., of an excitation to one of the spurious virtual

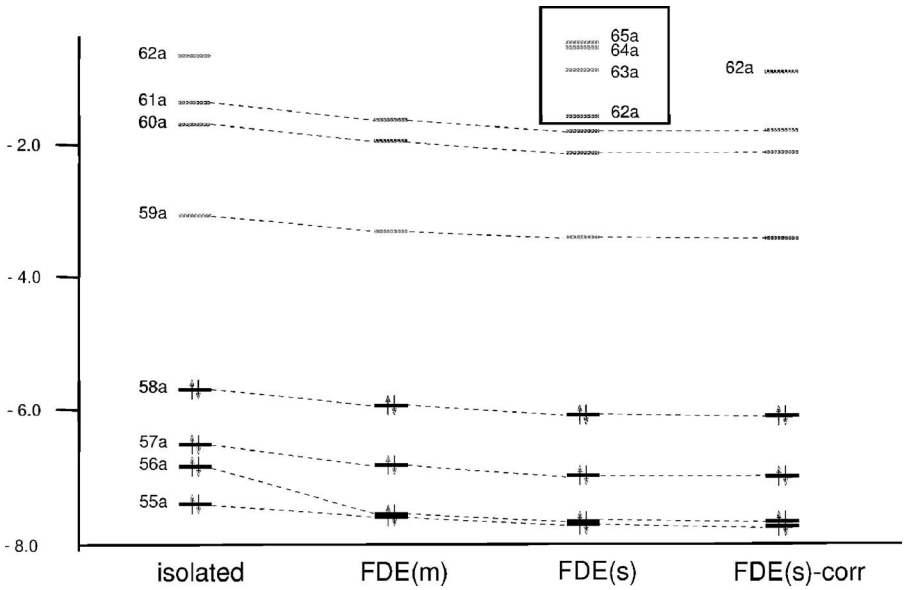

FIG. 8. Orbital energies (in eV) of the relevant orbitals calculated for aminocoumarin C151 surrounded by 30 water molecules. Only orbitals with energies lower than −0.3 eV have been included. As reference, the orbital energies calculated for the isolated aminocoumarin C151 are shown first, together with those calculated both using FDE(m) and FDE(s). Finally, the orbital energies calculated in a FDE(s) calculation using the long-distance corrected approximation to v_T are given [labeled FDE(s)-corr]. See text for details.

orbitals, and the eighth excitation has a contribution of 69.4% of such an excitation. The excitation energies of both of these excitations appear in the energy range of interest and show a significant oscillator strength. In the FDE(m) calculation, no similar excitations are found.

VII. A LONG-DISTANCE CORRECTED APPROXIMATION TO v_T

To compensate for the wrong long-distance limit of the kinetic-energy component of the embedding potential, we can improve the currently available approximations, which employ Eq. (3) in combination with an approximate LDA or GGA kinetic-energy functional, by enforcing the correct long-distance limit. The strategy followed is similar to that applied in Refs. 52 and 53 to enforce the correct description of charge-transfer excitations in TDDFT.

To achieve the correct long-distance limit, we augment the approximate kinetic-energy component $\tilde{v}_T$ of the embedding potential with a correction term v_T^{corr}, i.e.,

$$\tilde{v}_T[\rho_{\mathrm{I}},\rho_{\mathrm{II}}](\boldsymbol{r}) = \left.\frac{\delta \tilde{T}_s[\rho]}{\delta\rho}\right|_{\rho=\rho_{\mathrm{tot}}(\boldsymbol{r})} - \left.\frac{\delta \tilde{T}_s[\rho]}{\delta\rho}\right|_{\rho=\rho_{\mathrm{I}}(\boldsymbol{r})} + v_T^{\mathrm{corr}}[\rho_{\mathrm{I}},\rho_{\mathrm{II}}](\boldsymbol{r}). \tag{33}$$

This correction term should enforce the correct long-distance limit at the frozen system. In all other cases, it should leave the approximate $\tilde{v}_T$ unchanged because it is expected to be a rather good approximation in those cases, and currently there are no better approximations available.

For this correction term, we therefore chose the form

$$\begin{aligned} v_T^{\mathrm{corr}}[\rho_{\mathrm{I}},\rho_{\mathrm{II}}](\boldsymbol{r}) &= -\exp\left[-\left(\frac{\rho_{\mathrm{I}}(\boldsymbol{r})}{\alpha\rho_{\mathrm{II}(\boldsymbol{r})}}\right)^2\right]\left(v_{\mathrm{nuc}}^{\mathrm{II}}(\boldsymbol{r}) + \int \frac{\rho_{\mathrm{II}}(\boldsymbol{r}')}{|\boldsymbol{r}-\boldsymbol{r}'|}d\boldsymbol{r}'\right. \\ &+ \left.\frac{\delta E_{\mathrm{xc}[\rho]}}{\delta\rho}\right|_{\rho=\rho_{\mathrm{tot}}(\boldsymbol{r})} - \left.\frac{\delta E_{\mathrm{xc}[\rho]}}{\delta\rho}\right|_{\rho=\rho_{\mathrm{I}}(\boldsymbol{r})} \\ &+ \left.\frac{\delta \tilde{T}_s[\rho]}{\delta\rho}\right|_{\rho=\rho_{\mathrm{tot}}(\boldsymbol{r})} - \left.\frac{\delta \tilde{T}_s[\rho]}{\delta\rho}\right|_{\rho=\rho_{\mathrm{I}}(\boldsymbol{r})}\Bigg). \end{aligned} \tag{34}$$

In this expression, the first factor serves as a switching function that turns on the correction when needed, but that is zero otherwise. When the correction is switched on, i.e., the exponential in the above expression equals 1, the term in parentheses, which equals the approximate effective embedding potential, is subtracted, thus leading to the total effective embedding potential being zero and enforcing the correct long-distance limit at the frozen subsystem. To decide when this correction is switched on, we used the ratio of $\rho_{\mathrm{I}}(\mathbf{r})$ and $\rho_{\mathrm{II}}(\mathbf{r})$ in the switching function; i.e., when $\rho_{\mathrm{II}}(\mathbf{r})$ is sufficiently large compared to $\rho_{\mathrm{I}}(\mathbf{r})$, the correction is switched on. Based on numerical tests, we chose a value of 0.1 for the parameter α, which means that the correction is applied when $\rho_{\mathrm{II}}(\mathbf{r})$ is ten times as large as $\rho_{\mathrm{I}}(\mathbf{r})$.

It should be noted that this proposed correction can only be applied if the initial assumptions given in Sec. IV are fulfilled, i.e., if the partitioning of the total electron density is such that the electron densities of the subsystems equal the ground-state densities of the separated subsystems. This is not the case if there is charge transfer between the subsystems. In such cases, the correction given above will enforce a long-distance limit that is not correct.

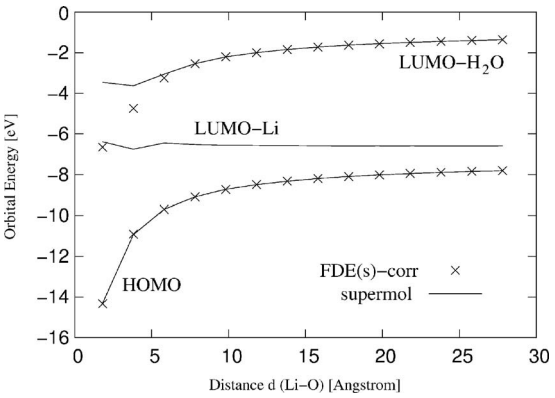

FIG. 9. Orbital energies calculated in FDE calculations on the H_2O subsystem in the presence of the frozen Li^+ subsystem using the PW91k kinetic-energy functional in combination with the long-distance correction as a function of the O–Li distance. As reference, the results of the supermolecular DFT calculation are also shown. See text for details.

The orbital energies calculated using this long-distance correction in combination with the PW91k kinetic-energy functional for the $H_2O\cdots Li$ complex studied above are shown in Fig. 9. It can be seen that while the orbital energy of the HOMO still agrees with the supermolecular HOMO, the spurious LUMO-Li found in the FDE(s) calculation does not appear anymore. Instead, the LUMO is given by an orbital localized at the H_2O subsystem, and its orbital energy agrees with the orbital energy of the LUMO-H_2O found in the supermolecular calculation.

Finally, we applied the correction in the calculation of aminocoumarin C151 surrounded by water. The orbital energies calculated in the FDE(s) calculation using the long-distance correction are included in Fig. 8. It can be seen that while the orbital energies of the other orbitals do not change significantly, the spurious virtual orbitals 62a–65a found in the uncorrected FDE(s) calculation, which were mainly localized at the water environment, do not appear anymore. Instead, there is only one virtual orbital 62a that was not present in the FDE(m) calculation.

An isosurface plot of this orbital is shown in Fig. 10. This virtual orbital is not localized at the water environment, but it is a N–H antibonding orbital of the amino group. A similar orbital is also present in the isolated molecule calculation (also shown in Fig. 10 for comparison). A closer inspection of the orbitals in the FDE(s) calculation shows that, actually, the virtual orbitals 62a, 64a, and 65a do also have a contribution from such a N–H antibonding orbital. The long-distance correction is thus able to remove the spurious contributions localized at the environment while keeping the contributions corresponding to virtual orbitals localized at the nonfrozen subsystem.

However, in the FDE(m) calculation such a N–H antibonding orbital appears only with a positive orbital energy. The long-distance correction compensates not only the attractive potential in the environment, but also the repulsive parts of the embedding potential. As the 62a orbital reaches out into regions of the environment where the embedding potential is mainly repulsive, this leads to a lowering of its orbital energy. If the long-distance correction is also applied in the FDE(m) calculation, a virtual orbital 62a similar to

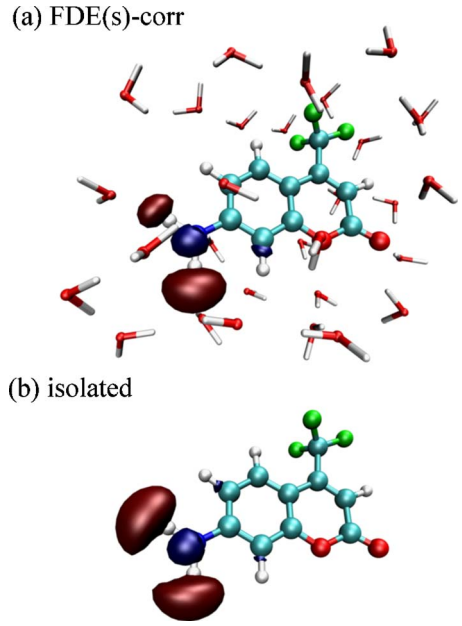

FIG. 10. (Color online) Isosurface plots (contour value: 0.05) of the unoccupied orbital 62a calculated for (a) aminocoumarin C151 surrounded by 30 water molecules using the long-distance corrected approximation to v_T in a FDE(s) calculation and (b) the isolated aminocoumarin C151. See text for details. Graphics: VMD. (Ref. 55).

that in the FDE(s) calculation is found at an orbital energy of −0.26 eV, which is still significantly higher than in the FDE(s) calculation. This remaining difference is due to the larger flexibility of the basis set in the FDE(s) calculation.

VIII. CONCLUSIONS

We have derived an exact expression for the kinetic-energy component v_T of the embedding potential that is used in the FDE scheme. By relating the functional derivative of the noninteracting kinetic-energy $T_s[\rho]$ to the KS potential $v_s[\rho]$ corresponding to this density, we obtain a way of calculating v_T exactly for an arbitrary pair of v_s-representable densities. In future work, this could be applied for performing FDE calculations using the exact kinetic-energy potential that could serve as a reference for developing improved approximations to v_T.

In this paper, we have applied the obtained expression to investigate v_T in the long-distance limit. We have shown that—under the assumption that the frozen electron density is close to the exact total electron density at the frozen subsystem—for large separations of the two subsystems the embedding potential at the nonfrozen subsystem should reduce to the purely electrostatic embedding potential, while at the frozen subsystem it should be zero.

One consequence of this exact limit is that for well-separated subsystems, not only the electron density and thus the occupied orbitals, but also the virtual orbitals are divided between the two subsystems; i.e., in the FDE calculation on one of the subsystems no virtual orbitals of the other subsystems should appear. This is a fundamental difference to pseudopotential approaches, in which only the occupied orbitals are projected out.

We have shown that while in the long-distance limit the approximations currently in use for v_T are correct at the nonfrozen subsystem, they fail at the frozen system, where the available GGA kinetic-energy functionals are not able to cancel the electrostatic and exchange-correlation components of the embedding potential. As our calculations on model systems have shown, this, in general, does not influence the calculated electron density and the calculated occupied orbitals, but it leads to artificially too low-lying virtual orbitals. These are problematic in two respects. First, as shown for $H_2O\cdots Li$, their orbital energy can drop below that of the HOMO, leading to nonaufbau solutions. Second, these spurious virtual orbitals will influence the calculation of response properties, for which a good description of virtual orbitals is crucial.

While it is in many cases possible to avoid these problems by not including basis functions on the frozen subsystem in the calculation of the nonfrozen subsystem [FDE(m)], these basis functions might be necessary to accurately describe hydrogen bonds between the subsystems, or diffuse basis functions on the nonfrozen subsystem might be able to probe the regions in which the embedding potential is wrong. In these cases, we recommend the use of the long-distance correction proposed in this work.

However, while the proposed long-distance correction is able to remove the spurious virtual orbitals in the model systems studied here, its applicability is rather limited. First, it can only be used if the partitioning is such that the subsystem densities are close to the ground-state densities of the well-separated subsystems, and it will, therefore, not work if there is a (partial) charge transfer from the nonfrozen to the frozen subsystem. It might be possible to devise more advanced corrections that detect such cases, e.g., by monitoring the orbital energies of both subsystems. Second, the proposed correction does only work in combination with approximate kinetic-energy functionals that are wrong in the long-distance limit. If it is used with the exact kinetic-energy functional, the correction of Eq. (34) will still give nonzero contributions. And third, the kinetic-energy component of the embedding potential obtained with this correction cannot be expressed as the functional derivative of an energy functional. For these reasons, this correction can only viewed as a first step toward more advanced approximations that ensure the correct long-distance limit.

Furthermore, the fact that the available approximations to v_T fail completely at the frozen subsystem makes it very likely that they can be considerably improved in the regions where the densities of the two subsystems overlap. The correction proposed in this work can be seen as a first step towards a new generation of approximations, which do not employ Eq. (3), i.e., which make use of an approximate kinetic-energy functional but that approximate v_T directly and which are constructed such that they obey the exact limits derived here. This might possibly be a promising route on the way to approximations that will also be applicable in the case of stronger interactions and thus remove some of the limitations the FDE scheme currently still has.

ACKNOWLEDGMENTS

The authors thank The Netherlands Organization for Scientific Research (NWO) for financial support via the TOP and Vici programs. The authors are grateful to Tomasz Wesolowski and Marcin Dulak (Geneva) for verifying the results obtained for $H_2O\cdots Li^+$ using their implementation of FDE in the DEMON2K program package.

[1] T. A. Wesolowski and A. Warshel, J. Phys. Chem. **97**, 8050 (1993).
[2] T. A. Wesolowski, in *Computational Chemistry: Reviews of Current Trends*, edited by J. Leszczynski (World Scientific, Singapore, 2006), Vol. 10.
[3] J. Neugebauer, M. J. Louwerse, E. J. Baerends, and T. A. Wesolowski, J. Chem. Phys. **122**, 094115 (2005).
[4] J. Neugebauer, Ch. R. Jacob, T. A. Wesolowski, and E. J. Baerends, J. Phys. Chem. A **109**, 7805 (2005).
[5] Ch. R. Jacob, J. Neugebauer, L. Jensen, and L. Visscher, Phys. Chem. Chem. Phys. **8**, 2349 (2006).
[6] J. Neugebauer, M. J. Louwerse, P. Belanzoni, T. A. Wesolowski, and E. J. Baerends, J. Chem. Phys. **123**, 114101 (2005).
[7] Ch. R. Jacob and L. Visscher, J. Chem. Phys. **125**, 194104 (2006).
[8] J. Neugebauer and E. J. Baerends, J. Phys. Chem. A **110**, 8786 (2006).
[9] M. Štrajbl, G. Hong, and A. Warshel, J. Phys. Chem. B **106**, 13333 (2002).
[10] M. H. M. Olsson, G. Hong, and A. Warshel, J. Am. Chem. Soc. **125**, 5025 (2003).
[11] J. Neugebauer, J. Chem. Phys. **126**, 134116 (2007).
[12] N. Govind, Y. A. Wang, A. J. R. da Silva, and E. A. Carter, Chem. Phys. Lett. **295**, 129 (1998).
[13] N. Govind, Y. A. Wang, and E. A. Carter, J. Chem. Phys. **110**, 7677 (1999).
[14] T. Klüner, N. Govind, Y. A. Wang, and E. A. Carter, Phys. Rev. Lett. **86**, 5954 (2001).
[15] T. Klüner, N. Govind, Y. A. Wang, and E. A. Carter, J. Chem. Phys. **116**, 42 (2002).
[16] P. Huang and E. A. Carter, J. Chem. Phys. **125**, 084102 (2006).
[17] Y. A. Wang and E. A. Carter, in *Theoretical Methods in Condensed Phase Chemistry*, edited by S. D. Schwartz (Kluwer, Dordrecht, 2000), Chap. 5, pp. 117–184.
[18] F. Tran and T. A. Wesolowski, Int. J. Quantum Chem. **89**, 441 (2002).
[19] T. A. Wesolowski, H. Chermette, and J. Weber, J. Chem. Phys. **105**, 9182 (1996).
[20] T. A. Wesolowski, J. Chem. Phys. **106**, 8516 (1997).
[21] T. A. Wesolowski, Y. Ellinger, and J. Weber, J. Chem. Phys. **108**, 6078 (1998).
[22] J. P. Perdew, in *Electronic Structure of Solids*, edited by P. Ziesche and H. Eschrig (Akademie Verlag, Berlin, 1991), p. 11.
[23] A. Lembarki and H. Chermette, Phys. Rev. A **50**, 5328 (1994).
[24] T. A. Wesolowski, P.-Y. Morgantini, and J. Weber, J. Chem. Phys. **116**, 6411 (2002).
[25] T. A. Wesolowski and F. Tran, J. Chem. Phys. **118**, 2072 (2003).
[26] Ch. R. Jacob, T. A. Wesolowski, and L. Visscher, J. Chem. Phys. **123**, 174104 (2005).
[27] T. A. Wesolowski, J. Am. Chem. Soc. **126**, 11444 (2004).
[28] M. Iannuzzi, B. Kirchner, and J. Hutter, Chem. Phys. Lett. **421**, 16 (2006).
[29] E. V. Stefanovich and T. N. Truong, J. Chem. Phys. **104**, 2946 (1995).
[30] M. Dułak and T. A. Wesołowski, J. Chem. Phys. **124**, 164101 (2006).
[31] J. P. Perdew, K. Burke, and M. Ernzerhof, Phys. Rev. Lett. **77**, 3865 (1996).
[32] J. Tao, J. P. Perdew, V. N. Staroverov, and G. E. Scuseria, Phys. Rev. Lett. **91**, 146401 (2003).
[33] R. van Leeuwen and E. J. Baerends, Phys. Rev. A **49**, 2421 (1994).
[34] P. R. T. Schipper, O. V. Gritsenko, S. J. A. van Gisbergen, and E. J. Baerends, J. Chem. Phys. **112**, 1344 (2000).
[35] Y. A. Wang, N. Govind, and E. A. Carter, Phys. Rev. B **58**, 13465 (1998).
[36] Y. A. Wang, N. Govind, and E. A. Carter, Phys. Rev. B **60**, 16350 (1999).
[37] B. Zhou, V. L. Ligneres, and E. A. Carter, J. Chem. Phys. **122**, 044103 (2005).
[38] R. G. Parr and W. Yang, *Density-Functional Theory of Atoms and Mol-*

ecules (Oxford University Press, Oxford, 1989).
[39] J. D. Talman and W. F. Shadwick, Phys. Rev. A **14**, 36 (1976).
[40] P. Hohenberg and W. Kohn, Phys. Rev. **136**, B864 (1964).
[41] Q. Zhao, R. C. Morrison, and R. G. Parr, Phys. Rev. A **50**, 2138 (1994).
[42] Y. Wang and R. G. Parr, Phys. Rev. A **47**, R1591 (1993).
[43] J. P. Perdew, R. G. Parr, M. Levy, and J. L. Balduz, Jr., Phys. Rev. Lett. **49**, 1691 (1982).
[44] ADF, Amsterdam density functional program, Theoretical Chemistry, Vrije Universiteit Amsterdam, 2006 (http://www.scm.com).
[45] G. te Velde, F. M. Bickelhaupt, E. J. Baerends, C. Fonseca Guerra, S. J. A. van Gisbergen, J. G. Snijders, and T. Ziegler, J. Comput. Chem. **22**, 931 (2001).
[46] J. P. Perdew, J. A. Chevary, S. H. Vosko, K. A. Jackson, M. R. Pederson, D. J. Singh, and C. Fiolhais, Phys. Rev. B **46**, 6671 (1992).
[47] M. Dulak and T. Welosowski (private communication).
[48] A. Laio, J. VandeVondele, and U. Rothlisberger, J. Chem. Phys. **116**, 6941 (2002).
[49] R. Poteau, I. Ortega, F. Alary, A. Solis, J.-C. Barthelat, and J.-P. Daudey, J. Phys. Chem. A **105**, 198 (2001).
[50] R. Poteau, F. Alary, H. Abou El Makarim, J.-L. Heully, J.-C. Barthelat, and J.-P. Daudey, J. Phys. Chem. A **105**, 206 (2001).
[51] R. Kevorkyants, M. Dulak, and T. A. Wesolowski, J. Chem. Phys. **124**, 024104 (2006).
[52] O. Gritsenko and E. J. Baerends, J. Chem. Phys. **121**, 655 (2004).
[53] J. Neugebauer, O. Gritsenko, and E. J. Baerends, J. Chem. Phys. **124**, 214102 (2006).
[54] ADF-GUI, Scientific Computing and Modeling, Amsterdam, 2006 (http://www.scm.com).
[55] W. Humphrey, A. Dalke, and K. Schulten, J. Mol. Graphics **14**, 33 (1996).